JACS
JOURNAL OF THE AMERICAN CHEMICAL SOCIETY

COMMUNICATION

pubs.acs.org/JACS

# pH-Operated Mechanized Porous Silicon Nanoparticles

Min Xue,[†,§] Xing Zhong,[†,§] Zory Shaposhnik,[‡,§] Yongquan Qu,[†] Fuyuhiko Tamanoi,[‡] Xiangfeng Duan,[*,†] and Jeffrey I. Zink[*,†]

[†]Department of Chemistry and Biochemistry, [‡]Department of Microbiology, Immunology, and Molecular Genetics, University of California, Los Angeles, California 90095, United States

Supporting Information

**ABSTRACT:** Porous silicon nanoparticles (PSiNPs) were synthesized by silver-assisted electroless chemical etching of silicon nanowires generated on a silicon wafer. The rod-shaped particles (200−400 nm long and 100−200 nm in diameter) were derivatized with a cyclodextrin-based nanovalve that was closed at the physiological pH of 7.4 but open at pH <6. Release profiles in water and tissue culture media showed that no cargo leaked when the valves were closed and that release occurred immediately after acidification. In vitro studies using human pancreatic carcinoma PANC-1 cells proved that these PSiNPs were endocytosed and carried cargo molecules into the cells and released them in response to lysosomal acidity. These studies show that PSiNPs can serve as an autonomously functioning delivery platform in biological systems and open new possibilities for drug delivery.

Porous silicon-based materials have attracted much recent interest for bioapplications including sensing, imaging, and drug delivery.[1−6] Particles of porous silicon with the attractive properties of high surface area,[7,8] intrinsic luminescence, and biodegradability[1a,2−4,11] have become a very promising scaffold for delivering drugs. Polymer-coated porous silicon nanoparticles (PSiNPs) have been shown to be an effective chemotherapeutic drug delivery system.[1a] The method for drug transportation in these studies was based on the electrostatic interaction and/or physical adsorption of specific drugs to the particles.[1−4] A key challenge for drug delivery applications is to utilize and control the access to the pores of the PSiNPs in order to generate a stimulus-responsive system that can transport and release the payload on demand without premature release. Similar efforts involving mesoporous silica nanoparticles (MSNPs) have led to the development of molecular nanovalves that control the pore openings.[9] Because the surface of the PSiNPs is usually terminated with a native silica layer, it is reasonable to expect that nanovalve-controlled systems similar to those that have been developed on silica nanoparticles can also be adapted to the PSiNP platform. In this communication, we demonstrate the first example of a mechanized PSiNP system wherein access to the pore structure is controlled by nanovalves chemically bonded to the surface of the PSiNPs. We further show that these PSiNPs can be used as an in vitro delivery system to human pancreatic carcinoma PANC-1 cells, with the cargo being confined in the particles at pH 7.4 and released only upon exposure to the decreased pH in endocytic vesicles.

Traditionally, porous silicon is produced by applying a voltage bias to a silicon wafer in solutions containing hydrofluoric acid.[10] In this study, the rodlike PSiNPs were prepared by breaking down porous silicon nanowires (PSiNWs) that were generated on a silicon wafer via a Ag-assisted electroless chemical etching method.[8] To date, several mechanisms have been proposed to explain the porosification process.[8c,11,12] The mechanism suggested here, which is based on our previous work,[8c] is schematically illustrated in Figure 1A. Silver nanoparticles that were predeposited on the silicon wafer (1 in Figure 1A) etch pits into the wafer. The nanowires are consequently formed as the result of the pit walls left between particles. In the process, the Ag nanoparticles at the bottom of these pits can redissolve in the etching solution, diffuse up and nucleate again on the sidewalls of the as-formed silicon nanowires (2 and 3 in Figure 1A), serving as a new etching site and generating the pores (4 in Figure 1A). With this method, PSiNWs can be generated without external electricity, and the nanowire lengths as well as their pore sizes can be easily tuned by controlling the reaction time and other conditions.[8c] Figure 1B displays a cross-sectional scanning electron microscopy (SEM) image of an as-prepared PSiNW array on the substrate. The length of the nanowires was ∼30 $\mu$m. The nanowires were separated from the substrate and broken into small fragments via sonication to form PSiNPs (5 in Figure 1A). PSiNPs with different sizes were then separated using filtration membranes. The size chosen for this study was 200−400 nm, which was suitable for conducting in vitro studies. Figure 1C shows a transmission electron microscopy (TEM) image of PSiNPs after sonication, from which their average length was estimated to be ∼300 nm, in agreement with the result obtained from dynamic light scattering (DLS) measurements (Figure S2 in the Supporting Information). The pore structure was clearly observed using high-resolution TEM (HRTEM) (Figure 1C inset). $N_2$ adsorption−desorption analysis gives a BET surface area of 293 $m^2/g$ and a pore volume of 0.98 $cm^3/g$, consistent with a previous report.[8c] These PSiNPs exhibited a relatively wide pore size distribution (Figure S1) as a result of the varying sizes of the nucleated Ag nanoparticles on the sidewalls of the silicon nanowires.

In this study, a well-established pH-responsive nanovalve system consisting of an aromatic amino group and a cyclodextrin cap[9d,f] was chosen to be adapted to the PSiNPs. This nanovalve was shown to be tightly closed at the physiological pH of 7.4 and to open autonomously under the acidic conditions (pH <6) present in endosomal/lysomal vesicles. In order to attach the

**Received:** February 9, 2011
**Published:** May 19, 2011





dx.doi.org/10.1021/ja201252e | J. Am. Chem. Soc. 2011, 133, 8798–8801

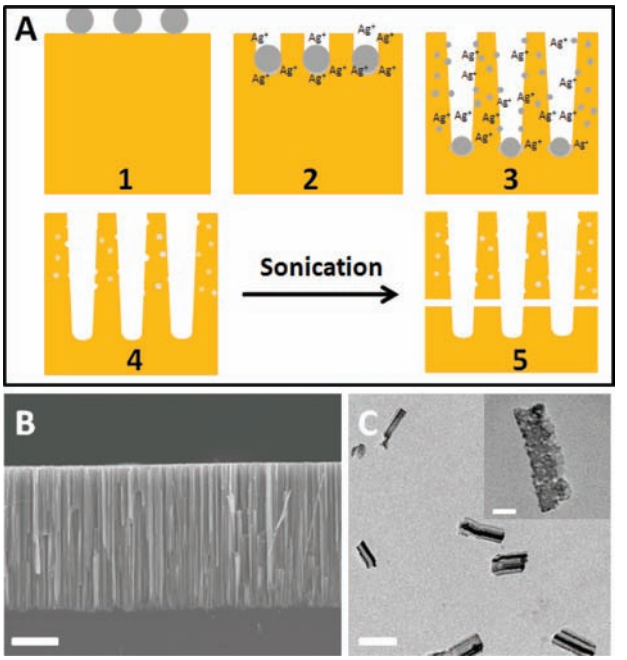


**Figure 1.** (A) Scheme of the formation of porous silicon nanowires by Ag-assisted electroless chemical etching method. (B) Cross-sectional SEM image of a porous silicon nanowire array on the substrate (scale bar = 10 $\mu$m). (C) TEM image of the PSiNPs after sonication and filtration (scale bar = 300 nm). The inset shows an HRTEM image of a PSiNP (scale bar = 50 nm).

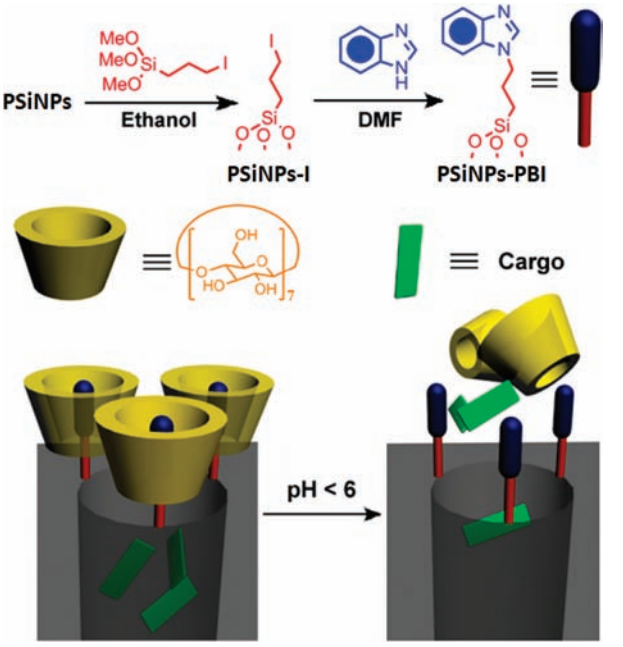


**Figure 2.** Schematic illustration of the synthesis and operation mechanism of the nanovalve. (top left) Attachment of the stalk precursor to the nanoparticle. (top right) Completion of the synthesis of the stalk. (bottom) Binding of the $\beta$-cyclodextrin cap to the neutral stalk (left) and release of the cap upon protonation of the stalk (right).

nanovalves, the PSiNPs were first derivatized with 3-iodopropyltrimethoxysilane and then coupled with a benzimidazole molecule under base catalysis (Figure 2). The solid-state NMR spectrum (Figure S3) proved that the modification was successful. The modified PSiNPs exhibited a BET surface area of 282 $m^2/g$ and a pore volume of 0.95 $cm^3/g$, which are similar to the values before the modification.

In order to demonstrate the operation of the nanovalves, the fluorescent biological staining dye Hoechst 33342 was chosen as a model cargo. The PSiNPs were loaded with the dye by soaking them in a concentrated Hoechst 33342 solution. $\beta$-Cyclodextrin was then added to the solution to finish the full assembly of the nanovalves, and this was followed by washing with water to remove dye molecules absorbed on the nanoparticles' exteriors. Under neutral pH conditions, the benzimidazole stalk remains hydrophobic and therefore can bind to the cyclodextrin molecule via supramolecular interactions. As a result, the bulky cyclic cyclodextrin molecules block the pore openings and function as gatekeepers to prevent the cargo in the pore from leaking out. When the pH is lowered, the benzimidazole is protonated, and the stalk−cyclodextrin binding constant decreases dramatically, causing the cyclodextrin to dissociate from the stalk. After the pores are unblocked, the cargo can diffuse out (Figure 2).

In order to verify the functional operation of the nanovalves, the cargo-loaded PSiNPs were placed in water, and the pH was lowered to stimulate the opening of the nanovalves. The increased concentration of cargo dye released into the aqueous solution was monitored as a function of time by fluorescence spectroscopy, generating a release profile (Figure 3A). Similar to the behavior in the case of MSNPs,[9f] these nanovalves on PSiNPs remained tightly closed at pH 7.0, giving a flat baseline as illustrated in Figure 3A. When the pH was lowered, the nanovalves opened and released the cargo. Cargo release was completed in about 3 h, which is much faster than in the case of MCM-41. As a control experiment, PSiNPs with stalks but no capping components were used. In this case, all of the cargo should have been removed from the PSiNPs during washing. The flat profile observed for these PSiNPs upon acidification showed that no cargo was released, as expected (Figure 3A).

The loading capacity of these PSiNPs was dependent on the size of the cargo. In the case of Hoechst 33342, a loading capacity of 1% (w/w) was determined using UV−vis absorption spectroscopy. This relatively low value was due to the small size of the Hoechst dye molecules. The nanovalve on the PSiNPs has a size of ~1.5 nm and thus is capable of controlling the release of Hoechst dye only from pores with sizes of <5.5 nm.[13]

Before conducting in vitro studies, it was important to verify that the nanovalve-modified PSiNPs remained functional under biological conditions, where the large amounts of buffering salt and proteins could potentially change the behavior of the nanovalves. In order to address this point, release profiles were generated in a DMEM cell culture medium containing 10% fetal bovine serum using Hoechst-loaded PSiNPs (Figure 3B). The PSiNPs were stable in the cell culture medium for at least 5 h, as no cargo leakage was observed. When the pH was lowered, the fluorescence intensity increased over time, indicating that the valves opened and released the cargo. This result demonstrates that the nanovalve-modified PSiNPs are stable, functional, and suitable for utilization as a drug delivery system.

Human pancreatic carcinoma PANC-1 cells were studied in order to prove that the nanovalve-modified PSiNPs can be taken up by cells and deliver their cargo inside them. The cells were incubated at 37 °C with fluorescein-labeled PSiNPs that were loaded with Hoechst 33342. Figure 4A shows that after incubation for 3 h, the Hoechst dye was released and stained the cell


dx.doi.org/10.1021/ja201252e | J. Am. Chem. Soc. 2011, 133, 8798–8801

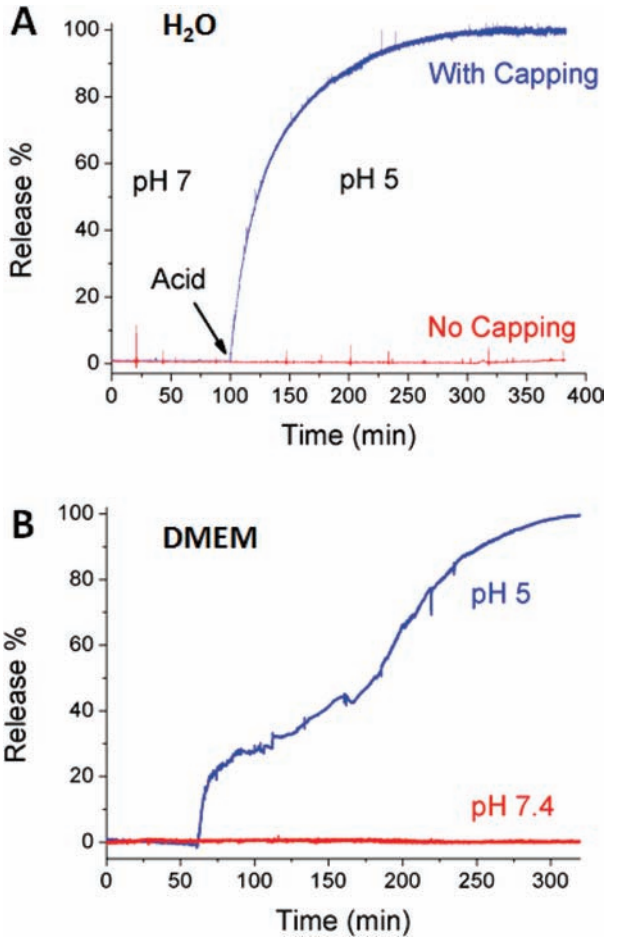


**Figure 3.** (A) Plot of the release of Hoechst 33342 from PSiNPs in aqueous solution. Acid was added to adjust the solution pH. The red line shows the release profile from the control experiment in which no cyclodextrin was used for capping. (B) Release profile generated in DMEM tissue culture medium. The blue line shows the functioning of the nanovalve when acid was added at 60 min. The red line shows the absence of leakage when the pH was unchanged.

nucleus. This process was relatively fast and consistent with the abiotic release profile. In order to further prove that it was the endocytosed PSiNPs that opened and released the dye, several control experiments were conducted. First, the cells were incubated with the same amount of PSiNPs at 4 °C, where the energy-dependent endocytosis pathway was inactive. In principle, if the nanovalves were controlling the release of the dye, then nonendocytosed PSiNPs would not stain the cells because they would not experience a pH change. As shown in Figure 4B, no staining was observed after incubation for 3 h at low temperature, proving that the dye was not released. Furthermore, contact between the PSiNPs and the cell membrane did not cause the nanovalves to open. This result also suggests that the endocytosis process is necessary for opening of the nanovalves. Second, in order to further investigate the functioning of the mechanized PSiNPs, a competition experiment was conducted. The cells were treated with the same amount of Hoechst-loaded FITC-labeled PSiNPs and increasing amounts of plain PSiNPs with no payload or FITC labeling. If the particles were indeed taken up primarily via a specific energy-dependent uptake process, the amount of FITC-labeled particle uptake (and nuclear staining)

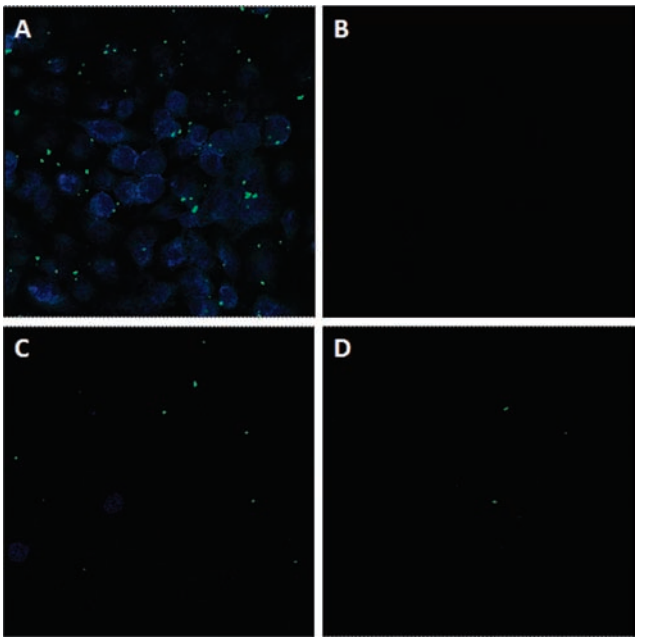


**Figure 4.** Confocal images of PANC-1 cells incubated with PSiNPs. (A) Cells treated with 20 $\mu$g/mL FITC-labeled PSiNPs loaded with Hoechst 33342 at 37 °C. (B) The same experiment conducted at 4 °C. No staining was observed after incubation at low temperature. (C, D) Competition tests: cells were treated with 20 $\mu$g/mL FITC-labeled PSiNPs loaded with Hoechst 33342 and (C) 60 or (D) 200 $\mu$g/mL of plain PSiNPs at 37 °C.

would decrease with increasing concentration of unlabeled particles. Figure 4C,D proves this assumption by showing much less FITC signal along with less nuclear staining. This result demonstrates that the nanovalves on the PSiNPs did not open in the cell culture medium at 37 °C and also proves that the endocytosis process was necessary to enable the particles to reach the lysosomes, triggering the release of the cargo.

In summary, we have demonstrated that pH-sensitive nanovalves can be successfully grafted onto the surface of PSiNPs and function as valves to control the pore openings. These mechanized PSiNPs can be endocytosed and release their cargo molecules inside cells. Further studies regarding control of larger-sized pores, optimization of the system, and understanding the biological process are in progress.

## ■ ASSOCIATED CONTENT

**Supporting Information.** Materials and methods used in the experiments, high-resolution TEM image of PSiNPs showing pore structures, $N_2$ adsorption−desorption isotherms, dynamic light scattering data, $^{13}C$ CPMAS NMR spectrum of the PSiNPs, fluorescence stability of the Hoechst 33342 dye, and pH-dependent release studies. This material is available free of charge via the Internet at http://pubs.acs.org.

## ■ AUTHOR INFORMATION

### Corresponding Author
xduan@chem.ucla.edu; zink@chem.ucla.edu

### Author Contributions
§These authors contributed equally.

## ■ ACKNOWLEDGMENT

This study was funded by the U.S. Public Health Service (Grant R01 CA133697), the U.S. Department of Defense (DTRA 1-08-1-0041), and the National Science Foundation (CHE 0809384). X.D. acknowledges support through the NIH Director's New Innovator Award Program, part of the NIH Roadmap for Medical Research, through Grant 1DP2OD004342-01.

## ■ REFERENCES

(1) (a) Park, J.-H.; Gu, L.; von Maltzahn, G.; Ruoslahti, E.; Bhatia, S. N.; Sailor, M. J. *Nat. Mater.* **2009**, *8*, 331–336. (b) Sailor, M. J.; Wu, E. C. *Adv. Funct. Mater.* **2009**, *19*, 3195–3208. (c) Cheng, L.; Anglin, E.; Cunin, F.; Kim, D.; Sailor, M. J.; Falkenstein, I.; Tammewar, A.; Freeman, W. R. *Br. J. Ophthalmol.* **2008**, *92*, 705–711. (d) Anglin, E. J.; Cheng, L.; Freeman, W. R.; Sailor, M. J. *Adv. Drug Delivery Rev.* **2008**, *60*, 1266–1277. (e) Wu, E. C.; Park, J.-H.; Park, J.; Segal, E.; Cunin, F.; Sailor, M. J. *ACS Nano* **2008**, *2*, 2401–2409.

(2) (a) Bimbo, L. M.; Sarparanta, M.; Santos, H. A.; Airaksinen, A. J.; Makila, E.; Laaksonen, T.; Peltonen, L.; Lehto, V.-P.; Hirvonen, J.; Salonen, J. *ACS Nano* **2010**, *4*, 3023–3032. (b) Salonen, J.; Laitinen, L.; Kaukonen, A. M.; Tuura, J.; Björkqvist, M.; Heikkilä, T.; Vähä-Heikkilä, K.; Hirvonen, J.; Lehto, V.-P. *J. Controlled Release* **2005**, *108*, 362–374.

(3) De Angelis, F.; Pujia, A.; Falcone, C.; Iaccino, E.; Palmieri, C.; Liberale, C.; Mecarini, F.; Candeloro, P.; Luberto, L.; de Laurentiis, A.; Das, G.; Scala, G.; Di Fabrizio, E. *Nanoscale* **2010**, *2*, 2230–2236.

(4) (a) Ferrati, S.; Mack, A.; Chiappini, C.; Liu, X.; Bean, A. J.; Ferrari, M.; Serda, R. E. *Nanoscale* **2010**, *2*, 1512–1520. (b) Tasciotti, E.; Liu, X.; Bhavane, R.; Plant, K.; Leonard, A. D.; Price, B. K.; Cheng, M. M.; Decuzzi, P.; Tour, J. M.; Robertson, F.; Ferrari, M. *Nat. Nanotechnol.* **2008**, *3*, 151–157. (c) Serda, R. E.; Ferrati, S.; Godin, B.; Tasciotti, E.; Liu, X. W.; Ferrari, M. *Nanoscale* **2009**, *1*, 250–259. (d) Serda, R. E.; Mack, A.; Pulikkathara, M.; Zaske, A. M.; Chiappini, C.; Fakhoury, J. R.; Webb, D.; Godin, B.; Conyers, J. L.; Liu, X. W.; Bankson, J. A.; Ferrari, M. *Small* **2010**, *6*, 1329–1340.

(5) Rosso-Vasic, M.; Spruijt, E.; Popovic, Z.; Overgaag, K.; van Lagen, B.; Grandidier, B.; Vanmaekelbergh, D.; Dominguez-Gutierrez, D.; De Cola, L.; Zuilhof, H. *J. Mater. Chem.* **2009**, *19*, 5926–5933.

(6) Vaccari, L.; Canton, D.; Zaffaroni, N.; Villa, R.; Tormen, M.; di Fabrizio, E. *Microelectron. Eng.* **2006**, *83*, 1598–1601.

(7) Hochbaum, A. I.; Gargas, D.; Hwang, Y. J.; Yang, P. D. *Nano Lett.* **2009**, *9*, 3550–3554.

(8) (a) Qu, Y. Q.; Zhong, X.; Li, Y. J.; Liao, L.; Huang, Y.; Duan, X. F. *J. Mater. Chem.* **2010**, *20*, 3590–3594. (b) Qu, Y. Q.; Liao, L.; Li, Y. J.; Zhang, H.; Huang, Y.; Duan, X. F. *Nano Lett.* **2009**, *9*, 4539–4543. (c) Zhong, X.; Qu, Y. Q.; Lin, Y. C.; Liao, L.; Duan, X. F. *ACS Appl. Mater. Interfaces* **2011**, *3*, 261–270.

(9) (a) Patel, K.; Angelos, S.; Dichtel, W. R.; Coskun, A.; Yang, Y. W.; Zink, J. I.; Stoddart, J. F. *J. Am. Chem. Soc.* **2008**, *130*, 2382–2383. (b) Nguyen, T. D.; Leung, K. C. F.; Liong, M.; Pentecost, C. D.; Stoddart, J. F.; Zink, J. I. *Org. Lett.* **2006**, *8*, 3363–3366. (c) Angelos, S.; Yang, Y. W.; Patel, K.; Stoddart, J. F.; Zink, J. I. *Angew. Chem., Int. Ed.* **2008**, *47*, 2222–2226. (d) Du, L.; Liao, S.; Khatib, H. A.; Stoddart, J. F.; Zink, J. I. *J. Am. Chem. Soc.* **2009**, *131*, 15136–15142. (e) Angelos, S.; Khashab, N. M.; Yang, Y. W.; Trabolsi, A.; Khatib, H. A.; Stoddart, J. F.; Zink, J. I. *J. Am. Chem. Soc.* **2009**, *131*, 12912–12914. (f) Meng, H.; Xue, M.; Xia, T.; Zhao, Y.-L.; Tamanoi, F.; Stoddart, J. F.; Zink, J. I.; Nel, A. E. *J. Am. Chem. Soc.* **2010**, *132*, 12690–12697.

(10) Cullis, A. G.; Canham, L. T.; Calcott, P. D. *J. Appl. Phys.* **1997**, *82*, 909–965.

(11) Chiappini, C.; Liu, X.; Fakhoury, J. R.; Ferrari, M. *Adv. Funct. Mater.* **2010**, *20*, 2231–2239.

(12) Huang, Z.; Geyer, N.; Werner, P.; de Boor, J.; Gösele, U. *Adv. Mater.* **2011**, *23*, 285–308.

(13) The size of the Hoechst molecule is about 2.5 nm × 0.75 nm. At the pore opening, the nanovalve occupies part of the space and blocks the pore. The size of nanovalve in this work was ~1.5 nm in diameter. If it is assumed that there were two nanovalves per pore opening, ~3 nm of the pore diameter would have been blocked. As a result, only pores with sizes smaller than 5.5 nm would have been utilized to trap Hoechst molecules. Any Hoechst dye stored in larger pores would have had enough space to move in and out freely and would have been removed from the PSiNPs during the washing process. When a larger molecule (doxorubicin) was used as the cargo, a loading capacity of 3% was determined under the same conditions.